POLYMER GEOMETRY AND Li$^+$ CONDUCTION IN POLY(ETHYLENE OXIDE)

L. Gitelman[1], M. Israeli[2]*, A. Averbuch[3], M. Nathan[4],

Z. Schuss[5], D. Golodnitsky[6]

[1] Faculty of Applied Mathematics, Technion, Haifa 32000, Israel

[2] Deceased February 18, 2007

[3] School of Computer Science, Tel Aviv University, Tel Aviv 69978, Israel

[4] School of Electrical Engineering, Tel Aviv University, Tel Aviv 69978, Israel

[5] Department of Mathematics, Tel Aviv University, Tel Aviv 69978, Israel

[6] School of Chemistry, Tel Aviv University, Tel Aviv 69978, Israel

November 29, 2007

---

*Prof. Moshe Israeli passed away on February 18, 2007. This paper is dedicated to his memory.

Abstract

We study the effect of molecular shape on Li^+ conduction in dilute and concentrated polymer electrolytes ($LiI : P(EO)_n (3 \le n \le 100)$). We model the migration-diffusion of interacting Li^+ ions in the helical PEO molecule as Brownian motion in a field of electrical force. Our model demonstrates that ionic conductivity of the amorphous PE structure is increased by mechanical stretching due to the unraveling of loops in the polymer molecule and to increased order. The enhancement of the ionic conductivity in the stretch direction, observed in our Brownian simulations, is in agreement with experimental results. We find an up to 40-fold increase in the $LiIP(EO)_7$ conductivity, which is also in agreement with experimental results. The good agreement with experiment lends much credibility to our physical model of conductivity.

1   Introduction

In this paper we refine our molecular model of lithium ion conduction in dilute and concentrated polymer electrolytes ($LiI : P(EO)_n (3 \le n \le 100)$) [1], by including additional geometrical features of the polymer molecule. The simplified stochastic model of ionic motion in [1] was based on an analogy between protein channels of biological membranes that conduct Na^+, K^+, and other ions, and the PEO helical chain that conducts Li^+ ions. The main simplification in [1] was the linear model of the PEO molecule, which was only allowed to form a random angle with the direction of the external force field. The present refinement of the model, the inclusion of circular loops in the otherwise linear structure of the polymer channel, leads to a much better agreement with experimental results than the model of [1].

The realization that conductivity is confined largely to amorphous polymer electrolytes above their glass transition temperature, and that this is related to a unique conduction mechanism involving the creation of free volume, arising from the dynamics of the polymer chains, led to design strategies for new polymer electrolytes in which crystallinity was suppressed and segmental motion maximized [5]. This in turn, led to some enhancement in ionic conductivity at room temperature. However, despite innovative designs of flexible polymers and the synthesis of salts containing asymmetric anions capable of suppressing crystallinity the ionic conductivity has been persistently limited to $10^{-4} \, S \, cm^{-1}$ at room temperature, which is insufficient for many lithium battery applications.

The view that ion transport in polymer electrolytes occurs in a structureless continuum of a random free volume is not entirely compatible with microscopic structure. In fact, polymer electrolytes are semicrystalline systems with crystalline regions linked by amorphous domains

composed of entangled and disentangled areas [6] and crystalline polymer-salt structures are available for only a few discrete compositions.

The PEO chains adopt a helical conformation with all $C - O$ bonds trans and $C - C$ bonds either gauche or gauche minus [8]. Each PEO chain is associated with a dedicated set of cations and anions that do not coordinate to any other chain. In other words, there are no ionic cross-links between chains; there are only weak van der Waals interactions. Typically, the composition of polymer-salt complex is $3 : 1$. Changing the polymer-salt ratio from $3 : 1$ to $1 : 1$ has a profound influence on the PE structure [8]. The polymer chain conformation changes from helical to a stretched zigzag arrangement and the cations are coordinated by only two ether oxygens and four anions. The anions coordinate simultaneously cations, which are themselves associated with different PEO chains. As a result, there is extensive inter-chain cross-linking in the $1 : 1$ complexes.

Increasing the polymer-salt ratio from $3 : 1$ to $6 : 1$ has an equally profound influence on the crystal structure (see [8]). The cations are arranged in rows, where each row is located within a cylindrical tunnel formed by two PEO chains. Each chain forms the surface of a half cylinder and the two chains interlock on each side to complete the cylindrical arrangement. The anions do not coordinate the cations, but are instead located outside the PEO cylinder in the inter-chain space. The anions are also arranged in rows.

On passing from the crystalline to the amorphous state, the structure is largely retained with only a loss of register between the chains, leading to disruption of the long range order [8]. In particular, it appears that the PEO chain retains its helical conformation while the cations remain inside the helices and are associated with their anions. The fact that in both $3 : 1$ and $6 : 1$ compositions the cations remain within tunnels defined by the PEO chains suggests that cation transport occurs preferentially along such tunnels, with the rate limiting step being transfer between tunnels, in agreement with [7]. The organization of the chains in a more aligned fashion (see Fig. 1B) facilitates transport along and between chains.
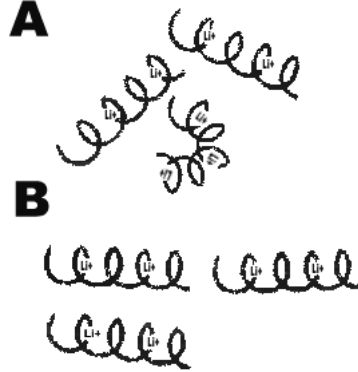
Figure 1: A: Disorganized and (B) organized models of a polymer electrolyte

Evidence supporting the view that organization of chains can be important for enhancing conductivity was presented in [12, 13, 14], where it was shown that ionic conductivity in the static ordered environment of the crystalline phase is greater than that in the equivalent amorphous materials above the glass transition point. Stretching of polymer electrolytes resulted in highly improved orientation of fibers in the $LiIP(EO)_n$ electrolytes with $3 < n < 100$ and in the enhancement of the longitudinal conductivity by a factor of $3 - 40$ ([12, 13, 14]) where n indicates that for each Li$^+$ ion there are n atoms of O in the PEO polymer electrolytes. It was found that the more amorphous the PE, the less its lengthwise conductivity is influenced by stretching. A model that accounts for stretching-induced structural anisotropy accompanied by ion conduction enhancement was introduced in [9]. It addresses a transition from spherical to spheroidal shapes of the high conduction regions as a result of alignment. The results of the present paper indicate that mechanical stretching affects not only the alignment of the polymer molecules, but also their geometrical conformation, as described below.

In this paper we extend the simulation developed in [1] to a more complicated geometry of the PEO. We add circular loops to the linear structure of the polymer (see 2), which causes a significant effect. This is due to the formation of a potential barrier by the external electrostatic field, when a lithium ion diffuses in the loop against the field. The presence of the barriers changes the time course of the ionic flow relative to that in a linear molecule. Two stages of ionic flow appear. First, there is depletion of the ions located on the down slope of the electric potential in the polymer and the accumulation of mobile ions in the potential wells. The Coulombic repulsion between the lithium ions forms a quasi-stationary energy landscape with shallow wells, which become deeper as the ionic concentration decreases, due to activated escapes over the barriers. Thus the ionic current decays exponentially in time in the last stages of conduction.
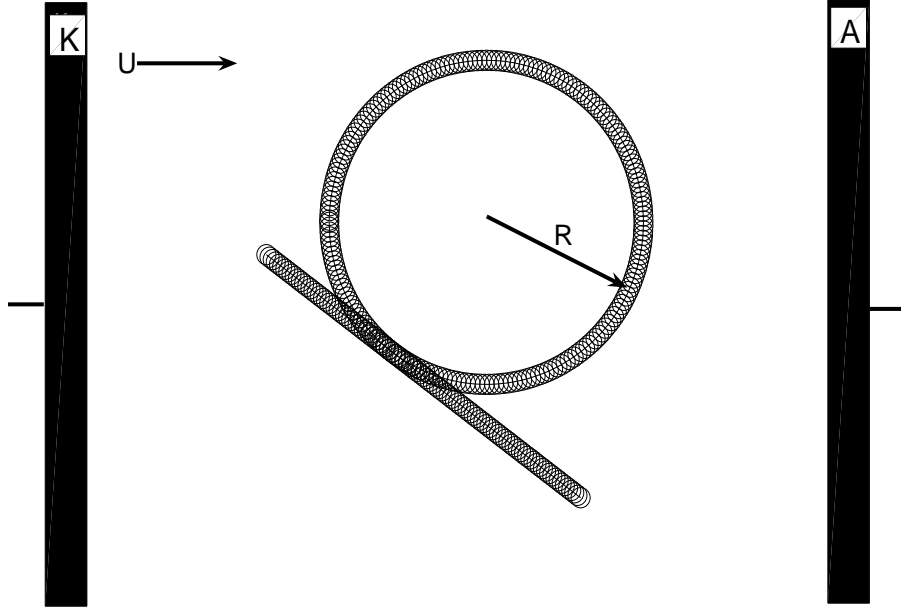
4

Figure 2: The polymer (part of the molecule) containing circular loop

The main effect of mechanical stretching of the assumed polymer structure on the ionic current is due to the geometrical effect: stretching decreases the radii of the loops and may even eliminate some of them altogether. This, in turn, changes the electric energy landscape for the diffusion of the ions: barriers are lowered or eliminated, so ionic motion becomes mostly drift and diffusion down the potential gradient, resulting in a dramatically increased conductivity of the stretched polymer. Our refined simulation reveals this distinct effect. The results of the simulations are given in Sections 3.2 and 4. The effect of heating, which is consistent with Kramers' theory of activation [25], is presented in Section 3.2.

2 The simulation model

We assume that the as-cast PEO under consideration consists of long helical chains of small radius, whose axes are oriented randomly. The axis of each chain is bent many times, forming a random helix. We consider one turn of such a helix and assume it is a circular loop. The random loop radius is assumed several times the random step of the helical turn. The axis of the random helix, which is essentially a bundle of loops, is inclined relative to the line perpendicular to the electrodes A and K, which are a distance L apart (see Fig. 3 for a single chain that

5

bridges the gap). The angle of inclination α is assumed uniformly distributed in the interval $0 \leq \alpha \leq \pi/2$.
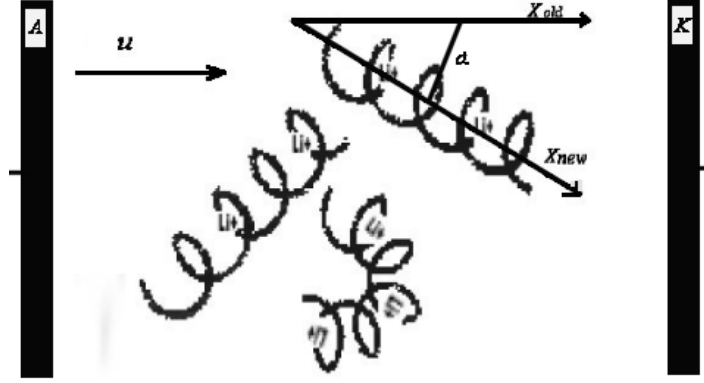

Figure 3: The helix (molecule) and the setup of the physical model

For $\alpha = 0$, the main Li$^+$ transport mechanism is diffusion and transport down the potential gradient inside the channel. For channels parallel to the electrodes ($\alpha = \pi/2$), the main mechanism is inter-channel cation hopping. For intermediate SPE chain geometries ($0 < \alpha < \pi/2$) the transport process is a mixture of intra-chain diffusion and migration and inter-chain hopping. The motion of the anions is migration and diffusion outside the helices. The diffusive motion of both lithium and iodine ions in the polymer matrix is due to the thermal motion of the polymer segments and chains. A comparison with laboratory experiments is done in [12]-[14].

The model of the motion of the mobile Li$^+$ ions is axial single file Brownian motion in an electric field of the polymer, the mobile ions and the external voltage. The polymer is represented as a combination of charge distribution, noise and dissipation. The solenoidal PEO helix, Fig. 4, is replaced ([23]) with a sequence of 2294 units of $CH_2 - CH_2 - O$, seven units of $CH_2 - CH_2 - O$ per two turns of the narrow helix (see Fig. 4). The length of two turns of the narrow helix is $d = 1.93$ nm. The units of CH_2 are at a distance $r_{CH} = 0.1nm$ from the x-axis, which is the axis of a linear segment of the narrow helix, and the units of O are at a distance $r_O = 0.04nm$ from the x-axis. Typical charge distribution values are $+0.245$ for a unit of CH_2

and -0.406 for a unit of O ([21]- [23]). The spatial structure of the PEO is that of a random helix formed by the narrow helix – see Fig. 3. We measure arclength s along the axis of the narrow helix and use it as a global coordinate of a lithium ion.
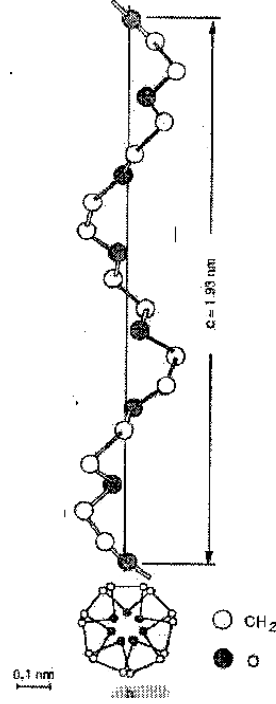

Figure 4: Schematic model of poly(ethylene oxide). The same two turns of the helix appear at the bottom of the figure

The Coulombic potential, created in a loop of radius R in a plane perpendicular to the electrodes at arclength s on the axis of the narrow helix by the PEO charges, is given by

$$\Phi(s) = \sum_{j=1}^{N} \left(\sum_{i=1}^{n_1} \frac{q^+}{\sqrt{4R^2 \sin^2 \left(\dfrac{s - s_{ij}^+}{2R} \right) + r_{CH}^2}} + \sum_{i=1}^{n_2} \frac{q^-}{\sqrt{4R^2 \sin^2 \left(\dfrac{s - s_{ij}^-}{2R} \right) + r_O^2}} \right), \quad (2.1)$$

where q^- and q^+ are the net negative and positive charges on a ring, s_{ij}^+ and s_{ij}^- are respectively the coordinates of the units CH_2 and O, and n_1 and n_2 are the numbers of positive and negative particles in the loop, respectively. The potential of an external constant field in a direction

7

perpendicular to the plane of the electrodes, created by an applied voltage, is

$$\Psi_E(s) = -\frac{V_A - V_K}{L} x \sin \eta = -ER \cos\left(\frac{s}{R}\right) \sin \eta,$$

where $E = \dfrac{V_A - V_K}{L}$ and η is the angle between the plane of the loop and the plane of the electrodes. We write the configuration space coordinates of the lithium and iodine ions respectively as

$$\boldsymbol{s} = (s_1, s_2, \ldots, s_L), \quad \boldsymbol{s}' = (s'_1, s'_2, \ldots, s'_L).$$

The potential of the electric field acting on the n-th lithium ion at s_n in the loop, including the Coulombic potential of the inter-ionic forces, is

$$\Psi_{Li^+}(\boldsymbol{s}, \boldsymbol{s}') = \sum_{i \neq n} \frac{q_{Li^+}}{2R \left| \sin\left(\frac{s_n - s_i}{2R}\right) \right|} + \sum_{i=1}^{L} \frac{q_{I^-}}{\sqrt{4R^2 \sin^2\left(\frac{s_n - s'_i}{2R}\right) + r_{CH}^2}} + \Phi(s_n) + \Psi_E(s_n)$$

and that of the force acting on the n-th iodine ion at s'_n is

$$\Psi_{I^-}(\boldsymbol{s}, \boldsymbol{s}') = \sum_{i=1}^{L} \frac{q_{Li^+}}{\sqrt{4R^2 \sin^2\left(\frac{s'_n - s_i}{2R}\right) + r_{CH}^2}} + \sum_{i \neq n} \frac{q_{I^-}}{2R \left| \sin\left(\frac{s'_n - s'_i}{2R}\right) \right|} + \Phi(s'_n) + \Psi_E(s'_n).$$

A more complex configuration consists of N linear segments of lengths S_i, inclined at angles $0 \leq \alpha_i \leq \pi/2$, $(i = 1, 2, \ldots, N)$, and $N - 1$ circular loops of radii R_i, attached at the ends of the linear segments at angles $0 \leq \eta_i \leq \pi/2$, $(i = 1, 2, \ldots, N - 1)$, respectively. The endpoints of the linear segments are the arclengths

$$\lambda_k = \sum_{i=1}^{k-1} S_i + 2\pi \sum_{i=1}^{k-1} R_i, \quad \mu_k = \sum_{i=1}^{k} S_i + 2\pi \sum_{i=1}^{k-1} R_i, \quad (k = 1, 2 \ldots, N)$$

and the arclengths in the loops are $\mu_k \leq s \leq \lambda_{k+1}$, $(k = 1, 2, \ldots, N - 1)$. Note that $\lambda_1 = 0$ and $\Psi_E(\lambda_1) = V_A$, and $\Psi_E(\lambda_{k+1}) = \Psi_E(\mu_k)$. The electric potential of the applied voltage is

$$\Psi_E(s) = \tag{2.2}$$

$$\begin{cases} -E(s - \lambda_k) \cos\alpha_k + \Psi_E(\lambda_k) & \text{if } \lambda_k \leq s \leq \mu_k, \ k = 1, \ldots, N \\[4mm] -ER_k \left[\cos\left(\frac{s - \mu_k}{R_k}\right) - 1\right] \sin\eta_k + \Psi_E(\mu_k) & \text{if } \mu_k < s \leq \lambda_{k+1}, \ k = 1, \ldots, N - 1. \end{cases}$$

The effect of mechanical stretching on the structure of the loops consists in decreasing the loops' radii R_k and the inclination angles α_k, as well as increasing the angles η_k to $\pi/2$. A simplified potential of the ion-ion Coulombic forces contains only interactions of ions that are in the same segment or the same loop. Thus the simplified potential of the electric field acting on the n-th lithium ion in the linear segment $\lambda_k \leq s_n \leq \mu_k$ is

$$\Psi_{Li^+}(\boldsymbol{s}, \boldsymbol{s}') = \sum_{\lambda_k \leq s_i \leq \mu_k, \ i \neq n} \frac{q_{Li^+}}{|s_n - s_i|} + \sum_{\lambda_k \leq s'_i \leq \mu_k} \frac{q_{I^-}}{\sqrt{(s_n - s'_i)^2 + r_{CH}^2}} + \Phi(s_n) + \Psi_E(s_n)$$

and that of the force acting on the n-th iodine ion at $\lambda_k \leq s'_n \leq \mu_k$ is

$$\Psi_{I^-}(\boldsymbol{s}, \boldsymbol{s}') = \sum_{\lambda_k \leq s_i \leq \mu_k} \frac{q_{Li^+}}{\sqrt{(s'_n - s_i)^2 + r_{CH}^2}} + \sum_{\lambda_k \leq s'_i \leq \mu_k, \ i \neq n} \frac{q_{I^-}}{|s'_n - s'_i|} + \Phi(s'_n) + \Psi_E(s'_n).$$

The simplified potential of the electric field acting on the n-th lithium ion in the loop $\mu_k \leq s_n \leq \lambda_{k+1}$ is

$$\Psi_{Li^+}(\boldsymbol{s}, \boldsymbol{s}') = \Phi(s_n) + \Psi_E(s_n) +$$

$$\sum_{\mu_k \leq s_i \leq \lambda_{k+1}, \ i \neq n} \frac{q_{Li^+}}{2R \left| \sin\left(\frac{s_n - s_i}{2R}\right) \right|} + \sum_{\mu_k \leq s'_i \leq \lambda_{k+1}} \frac{q_{I^-}}{\sqrt{4R^2 \sin^2\left(\frac{s_n - s'_i}{2R}\right) + r_{CH}^2}}$$

and that of the force acting on the n-th iodine ion at $\mu_k \leq s'_n \leq \lambda_{k+1}$ is

$$\Psi_{I^-}(\boldsymbol{s}, \boldsymbol{s}') = \Phi(s'_n) + \Psi_E(s'_n) +$$

$$\sum_{\mu_k \leq s_i \leq \lambda_{k+1}} \frac{q_{Li^+}}{\sqrt{4R^2 \sin^2\left(\frac{s'_n - s_i}{2R}\right) + r_{CH}^2}} + \sum_{\mu_k \leq s'_i \leq \lambda_{k+1}, \ i \neq n} \frac{q_{I^-}}{2R \left| \sin\left(\frac{s'_n - s'_i}{2R}\right) \right|}.$$

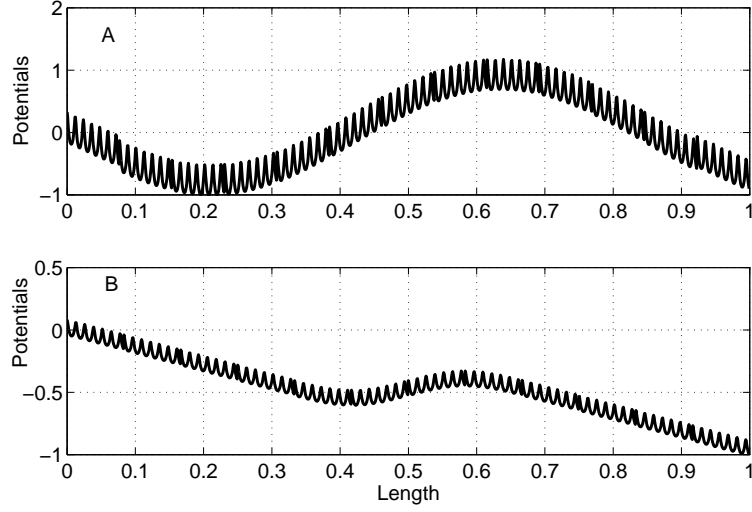Note that we assume that the I$^-$ ions are located at the distance r_{CH} from the axis.

Figure 5: The potential $\Phi(s) + \Psi_E(s)$ (eqs.(2.1), (2.2) for $N = 13$, $\alpha = 0$, $\eta = \pi/5$ (consisting of $N = 11$ for the loop and $N = 2$ for two line segments) in an unstretched (top) and for stretched (bottom) $N = 13$, $\alpha = 0$, $\eta = 0$ (consisting of $N = 4$ for the loop and $N = 9$ for two line segments). The local extrema of the potential correspond to the leftmost and rightmost points on the loop in fig. 2.

The random motion of the ions in the channel is described by the overdamped Langevin equations

$$
\begin{aligned}
\gamma_{Li}\dot{\boldsymbol{s}} &= \boldsymbol{F}_{Li}(\boldsymbol{s}, \boldsymbol{s}') + \sqrt{\frac{2\gamma_{Li}kT}{m_{Li}}}\,\dot{\boldsymbol{w}}_s, \\
\gamma_I\dot{\boldsymbol{s}}' &= \boldsymbol{F}_I(\boldsymbol{s}, \boldsymbol{s}') + \sqrt{\frac{2\gamma_I kT}{m_I}}\,\dot{\boldsymbol{\nu}}_s,
\end{aligned}
\tag{2.3}
$$

where $\dot{\boldsymbol{w}}_s$ and $\dot{\boldsymbol{\nu}}_s$ are vectors of independent standard δ-correlated Gaussian white noises, and the components of the electric forces (per unit mass) on the n-th lithium and iodine ions, respectively, are given by

$$
F_{Li}^{(n)}(\boldsymbol{s}, \boldsymbol{s}') = -q_{Li^+}\frac{\partial \Psi_{Li^+}(\boldsymbol{s}, \boldsymbol{s}')}{\partial s_n}
\tag{2.4}
$$

$$
F_I^{(n)}(\boldsymbol{s}, \boldsymbol{s}') = -q_{I^-}\frac{\partial \Psi_{I^-}(\boldsymbol{s}, \boldsymbol{s}')}{\partial s_n'}.
\tag{2.5}
$$

We simulate the system (2.3) by discretizing time and moving the ions according to the

Euler scheme

$$\boldsymbol{s}(t + \Delta t) \;\; = \;\; \boldsymbol{s}(t) + \frac{\boldsymbol{F}_{Li}(\boldsymbol{s}(t), \boldsymbol{s}'(t))}{\gamma_{Li}} \Delta t + \sqrt{\frac{2kT}{\gamma_{Li} m_{Li}}} \, \Delta \boldsymbol{w}_s(t),$$

$$\boldsymbol{s}'(t + \Delta t) \;\; = \;\; \boldsymbol{s}'(t) + \frac{\boldsymbol{F}_{I}(\boldsymbol{s}(t), \boldsymbol{s}'(t))}{\gamma_{I}} \Delta t + \sqrt{\frac{2kT}{\gamma_{I} m_{I}}} \, \Delta \boldsymbol{\nu}_s(t),$$

(2.6)

where $\Delta \boldsymbol{w}_s(t)$ and $\Delta \boldsymbol{\nu}_s(t)$ are zero mean independent Gaussian random variables with covariances $\boldsymbol{I}\Delta t$ ($\boldsymbol{I}$ is the unit matrix). A Li$^+$ trajectory $s_i(t)$, which reaches the graphite anode (in Fig. 3), is instantaneously restarted at $s_i = 0, \;\; i = 0, 1, ..., L$, and the counter of the restarted trajectories is increased by 1. An I$^-$ trajectory, which reaches either the cathode or anode, is instantaneously reflected. The total charge $Q(t)$ absorbed in the graphite in time t produces the noisy battery current

$$I(t) = \frac{dQ(t)}{dt}.$$

(2.7)

We simulate 16058 bound ions in each chain ([22]). The interactions between all charges are computed efficiently by a Fast Multipole Method (FMM)-type method [30]. Our aim is to calculate the steady-state average of $\langle I(t) \rangle$.

The shape of the simulated molecule is a single loop with two line segments, leading in and out of the loop and forming a random angle α with the external electric field. The radius of the loop is a fit parameter that was chosen to fit the experimental results at $n = 20$.

3 Experimental and simulation results

3.1 Experimental results in the literature

SEM observations together with XRD and FTIR studies of the $LiIP(EO)n$ PEs show that stretching the $LiIP(EO)20$ electrolyte converts a sample with a random distribution of helical crystalline microphases into a textured one. After removal of the load, stretched polymer electrolytes retained high ionic conductivity. This phenomenon is seen for semicrystalline complexes of poly(ethylene oxide) with different salts, such as lithium iodide, lithium trifluoromethanesulfonate, lithium hehafluoroarcenate and lithium triuoromethanesulfonimide (see [11, 12, 13, 14]). According to the FTIR results ([13]), a stretched polymer electrolyte adopts a modified helical structure similar to that of an extended salt-free PEO helix. In the aligned conformation of the helix, the oxygen atoms are directed inward, lining the tunnel cavity, and thus promoting cation transport. By using AC and DC conductivity measurements, it was demonstrated that

in spite of the formation of a more ordered PE structure and reduced segmental motion as a result of stretching, the ionic conductivity in the axial force direction increases by a factor of $2 - 40$, depending on the EO:Li ratio (n) and stretching conditions.

This has been attributed to fast cation migration within the helical channels, or anion transport outside, along the helical direction. The effect of uniaxial stress on the conductivity change in the amorphous P(EO) was found to be less pronounced (see [11, 13]). Alignment of the helical structural units is followed by a decrease in ionic conductivity normal to the direction of applied force.

The $10 - 15$-fold stretching-induced longitudinal conductivity enhancement observed in crystalline $Lil\ P(EO)_{20}$ electrolytes, and only sixfold conductivity increase in lithium trifluoromethanesulfonate PE indicates that aligned crystalline PEO chains are energetically more favorable for lithium ion transport than entangled chains.

3.2 Stretching results from simulation

It is a common belief [4, 28, 29, 26, 27] that ionic conductivity, which is the most important polymer electrolyte (PE) property, is higher in amorphous than in structured matrices, and that ion transport is mediated primarily by the motion of polymer segments. Despite this, in agreement with [7] and [11, 12, 13], we propose (see Section 1) that cation transport occurs preferentially along helices, with the limiting step rate being transfer between channels. A random arrangement of chains, such as might be envisaged in a simple amorphous (disordered) polymer (see Fig. 1A), is less conductive than a more ordered arrangement. Higher alignment between chains facilitates transport (see Fig. 1B). The above mentioned structural studies suggest that organization of chains should enhance ionic conductivity.

The two effects on the structural properties of the PEO contained in our model are (i) temperature increase and stretching, and (ii) ion-polymer interactions and ionic conductivity in dilute and concentrated states. We assume (Section 1 – Fig. 1) that the polymeric film is a thin layer of molecular structures (helices) with random orientations at random locations along axis (X_{old}). Moreover, each of the long helical chains is naturally bent many times, forming a random helix. We simplify the random helix to a bundle of loops, as described above (see Fig.3).

Upon mechanical stretching, the helices align along the axis of stretching. The inclination of most molecules in the PEO decreases and the loops are being flattened, i.e. the angles of inclination of the linear segments of the spirals and the radii of the loops decrease - see Fig. 1B. Mechanical stretching forms a more ordered PE structure which reduces the segmental motion,

that is, we transform the structure of the PEO from an amorphous state to a more crystalline state.

Figure 6 shows the graphs of the simulated conductivity and the conductivity measured in the direction of the applied force (see [14]) as a function of polymer electrolyte concentration. The dashed lines represent the simulation results for stretched (denoted "stretched".) and unstretched conductivity, and solid lines represent the experimental results. The curves of the plots of the ionic conductivity vs polymer electrolyte concentration are smoother than the experimental curves. As seen from the plots, the experimental ionic conductivity of the stretched as well as the unstretched polymer electrolytes at room-temperature (denoted RT) reaches a maximum at $n = 7$, just as in the simulated ionic conductivity at room-temperature (we disregard $n = 3$, because we do not have sufficient experimental data). From Fig. 6 we see that the stretching-induced DC conductivity increase depends on the $EO : Li$ ratio.

Figure 7 shows graphs of the simulated and measured conductivity at 65^oC (see [14]) as a function of polymer electrolyte concentration. According to the experimental data, the heating of the pristine PE films up to 65^oC is followed by an increase in the conductivity of the diluted electrolytes, whereas the simulation conductivity is increased for the concentrated ones as well.
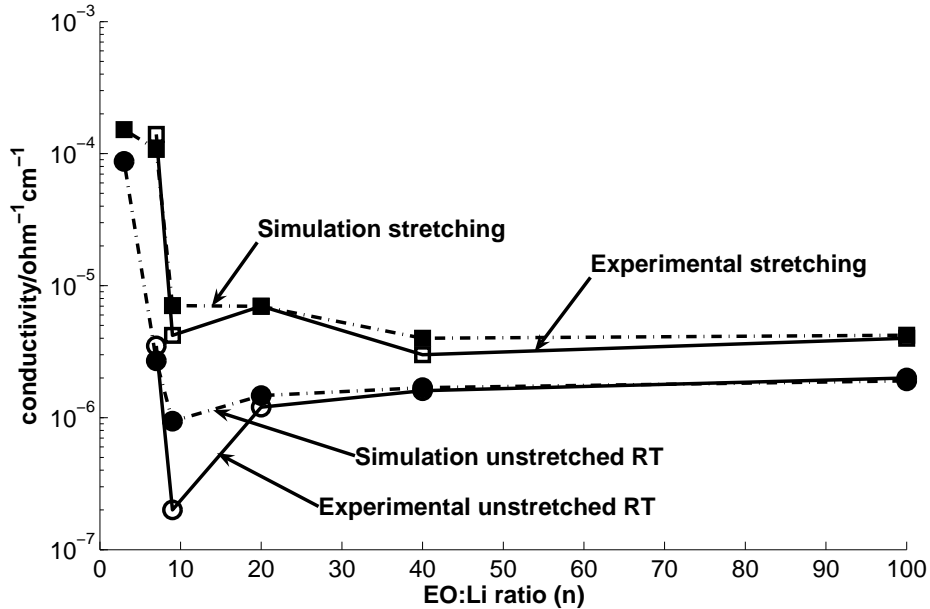

Figure 6: Simulation and experimental conductivity for different n as function of stretching at 60^oC. The experimental conductivity was measured after cooling of the stretched films to room-temperature .
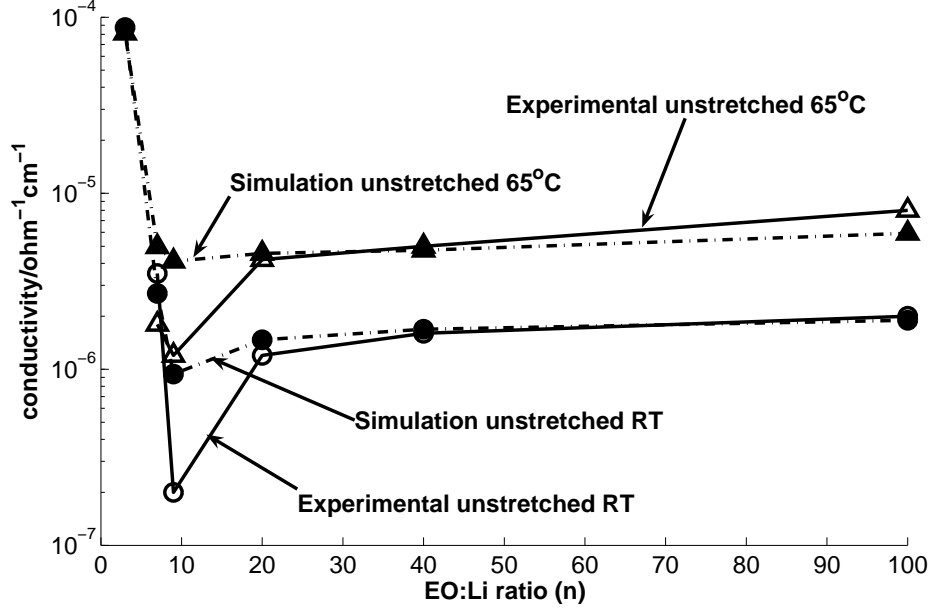
Figure 7: Simulation and experimental conductivity without stretching for different n as function of temperature.

When the curves in Fig. 6 are compared with those in Fig. 7, it is apparent that the stretching-induced longitudinal conductivity enhancement for the concentrated electrolytes is greater than that caused by heating.

The simulation and experimental data (see [13]) of the in-situ longitudinal DC conductivity measurements of dilute and concentrated $LiI\ P(EO)_n$ polymer electrolytes are shown in Figs. 8 and 9. The plots represent conductivity ratio vs n. The stretching process was found to influence the DC conductivity in the direction of the stretching more strongly than does an increase in temperature from 28° to 65^oC. The maximal conductivity enhancement (about 40-fold) in the direction of stretching was achieved in the $LiI\ P(EO)_7$ electrolyte with a highly elastic rubber-like structure. Temperature increase from room temperature to about the melting point of the PEO is followed by an almost 3-4-fold conductivity rise in dilute electrolytes. No significant changes were detected in concentrated systems.
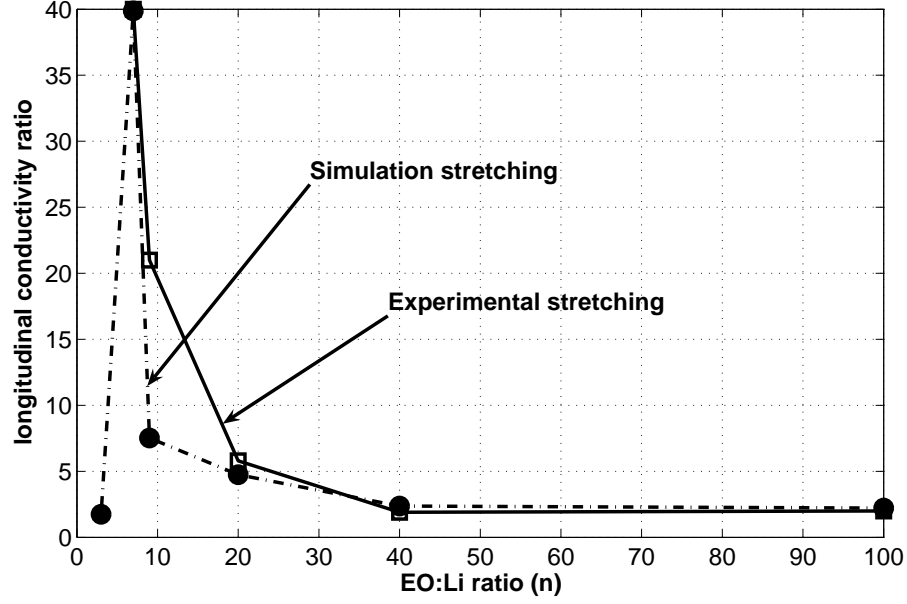
Figure 8: Simulation/experimental conductivity ratios for different n as function of n. The experimental stretching was at RT. All the experimental stretching has been done at ∼60C and the conductivity was measured both at RT and at 60C.
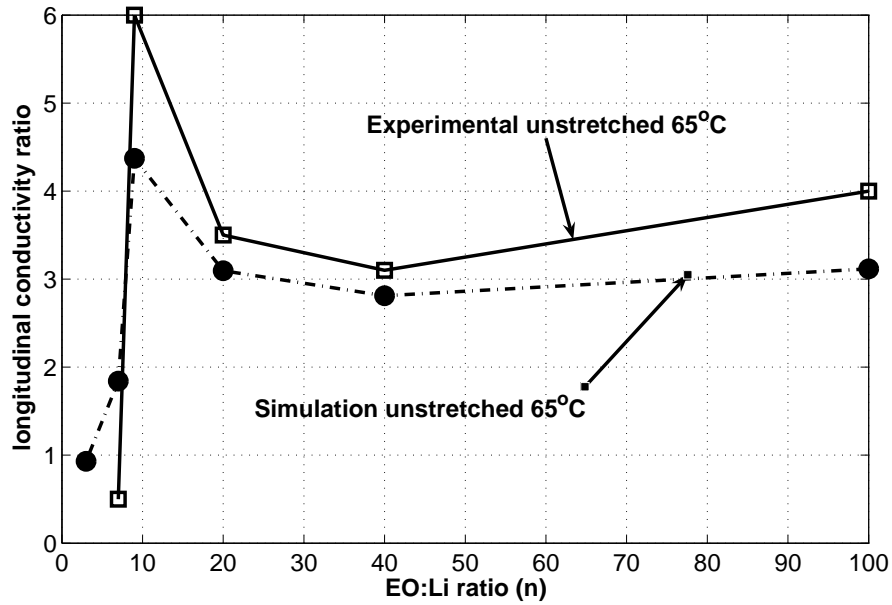

Figure 9: Simulation/experimental conductivity ratios for different n as function of n. It shows the effect of the temperature on the longitudinal conductivity of the unstretched LiI:P(EO)n solid polymer electrolytes (SPE)

The effect of stretching on the longitudinal conductivity of $LiI : P(EO)n$ solid polymer electrolytes (SPE) is summarized in Table 1.

EO:Li ratio (n)	Simulation results			Experimental results [13]-[14]		
	Unstr. σ (S/cm) $*10^{-6}$	Str. σ (S/cm) $*10^{-6}$	$\sigma_{str}/\sigma_{unstr}$ ratio	Unstr. σ (S/cm) $*10^{-6}$	Str. σ (S/cm) $*10^{-6}$	$\sigma_{str}/\sigma_{unstr}$ ratio
3	87.30	152.10	1.7			
7	2.70	107.67	39.9	2.6	100	38.0
9	0.94	7.07	7.5	0.4	4.3	12.0
20	1.47	6.97	4.7	1.0	7.0	7.0
40	1.69	4.00	2.4	1.6	2.9	1.8
100	1.90	4.21	2.2	2.0	4.3	2.2

Table 1: Effect of stretching on the longitudinal conductivity of $LiI : P(EO)n$ solid polymer electrolytes (SPE)

The effect of temperature on the longitudinal conductivity of unstretched $LiI : P(EO)n$ solid polymer electrolytes (SPE) is summarized in Table 2.

EO:Li ratio (n)	Simulation results			Experimental results [13]-[14]		
	σ at RT $*10^{-6}$	σ at T=65C $*10^{-6}$	σ_T/σ_{RT} ratio	σ at RT $*10^{-6}$	σ at T=65C $*10^{-6}$	σ_T/σ_{RT} ratio
3	87.30	81.13	0.9			
7	2.70	4.97	1.8	3.5	1.8	0.5
9	0.94	4.11	4.4	0.2	1.2	6.0
20	1.47	4.55	3.1	1.2	4.2	3.5
40	1.69	4.75	2.8	1.6	5	3.1
100	1.90	5.92	3.1	2	8	4.0

Table 2: Effect of temperature on the longitudinal conductivity of unstretched $LiI : P(EO)n$ solid polymer electrolytes (SPE)

4 Discussion and conclusions

Scanning Electron (SEM) and Atomic Force (AFM) microscopy, as well as FTIR and thermal measurements (DSC), show that stretching orders the structure of $LiI : P(EO)n$ polymer electrolytes [11]-[14]. Unidirectionally oriented fibrous microphases are clearly distinguishable in the SEM micrographs. The stretched polymer adopts a modified helical structure, similar to that of an extended salt-free PEO helix. In this configuration the CH_2 groups all face outward. This facilitates the onset of torsion in the polymer structure. In the aligned configuration of the helix the oxygen atoms are directed inward, lining the tunnel cavity and thus favoring cation transport.

We capture in our model this stretching-induced onset of order by representing the main geometrical features of the polymer molecule in terms of randomly oriented linear segments and circular loops which are transformed by stretching (see Fig. 3). Linear segments tend to align in the direction of stretching and the radii of circular loops decrease (see Fig. 1, B). The effect of conformational changes on conductivity is captured in our simplified model of Li^+/I^- motion. The ions, which interact electrostatically with the external field, the permanent charge of the polymer and with each other, are assumed to be Brownian particles in a field of force. The Li^+ ions are separated from the I^- ions by the polymer and from each other by Coulombic repulsion. Finite size effects (e.g., Lennard-Jones forces), which become significant only at high concentrations, are not incorporated in the present simulation.

The limitations of our model are due to its coarse-grained nature and to the heuristic way in which we choose orientations in space and the radii of the loops. This makes it difficult to assign volume fractions and local conductivities to a given material. Thus we cannot hope to account quantitatively for any observation, so our aim was to capture in our model mainly qualitative observations in a consistent way.

The simulation results show good agreement with experimental data of the effect of stretching on the longitudinal conductivity of PE over the entire range of n, except for $n = 9$ (Fig. 6 and Table 1). The agreement is not only in the correct trend (fast decrease from $n = 3$ to $n = 9$ with a further leveling of the conductivity to an almost constant value), but also in the absolute values of the conductivity, except for $n = 9$. Figure 6 and Table 1 show that the experimental ionic conductivity of the stretched and the unstretched polymer electrolyte at room-temperature goes through a minimum at $n = 9$, which is very much more pronounced than in the case of the simulation conductivity. This may be due to the difficulty in accounting exactly for the variation of the chemical structure of the polymer and the salt concentration. While the simulations accounts for the qualitative observations, the good agreement with ex-

perimental data at almost all salt-to-additive ratios supports the validity of our model.

We observe good agreement between the temperature effects in simulation and experiment over almost the entire salt-to-EO ratio range. Figures 7 and Table 2 show that the experimental ionic conductivity at room-temperature, as well as at $65^{o}C$, goes through a minimum at $n = 9$, which is very much more pronounced than in the case of the simulation data. In contrast, the agreement in the temperature effect on the PE longitudinal conductivity, shown in Fig. 9, is less impressive, though it has the correct trend. However, given the simplified model used in the simulation, the observed correct trend and absolute ratio values over the entire n range (as in Fig. 8 and as in Fig. 9) tends to support the validity of our model. A more detailed theoretical study of the model will be published separately.

Stretching seems to influence the conductivity in the direction of the force more strongly than the increase in temperature from RT to $65^{o}C$. The stretching-induced longitudinal conductivity enhancement found in more ordered polymer electrolyte hosts is attributed to fast cation migration within the helical channels. The maximum conductivity enhancement (about 40-fold) in the stretch direction found at $n = 7$ is attributed to highly aligned cylindrical tunnels for Li^{+} transport in double PEO chains coordinating the cations, as suggested in [8].

References

[1] L. Gitelman, M. Israeli, A. Averbuch, M. Nathan, Z. Schuss, D. Golodnitsky, *J. Comp. Phys.* **227**, pp.1162-1175 (2007)

[2] B. Scrosati, *Application of Electroactive Polymers,* Chapman and Hall, London, 1993.

[3] M. Nathan, D. Haronian, E. Peled, *Micro-electrochemical cell,* U. S. Patent 6,197,450.

[4] D. F. Shriver, P.G. Bruce, *Polymer Electrolytes I: General Principles, Solid State Electrochemistry, P.G. Bruce (Ed.)* Cambridge University Press, Great Britain, pp.95-119 (1995).

[5] F. M. Gray, *Polymer Electrolytes, RSC Materials Monographs,* The Royal Society of Chemistry, Cambridge, (1997).

[6] D. Lippits, S. Rastogi, G.W.H. Höhne, B. Mezari, P.C.M.M. Magusin, *Macromolecules* **40**, pp.1004-1010, (2007).

[7] M.B. Armand, *Ann. Rev. Matter Sci.* **16** (9-11), pp.245-261 (1986).

[8] Y.G. Andreev, P.G. Bruce, *Electrochimica Acta,* **45**, pp.1417-1423,(2000).

[9] O. Dürr, W. Dietrich, P. Maass, A. Nitzan, *Journal of Physical Chemistry B* **106** (24), pp.6149-6155 (2002).

[10] J.B. Kerr, *Lithium Batteries.* Science and Technology, Kluwer Academic Press, (G-A Nazri, G. Pistoia - Eds.) Boston, (2004)

[11] D. Golodnitsky, E. Livshits, Yu. Rozenberg, E. Peled, S. H. Chung, Y. Wang, S. Bajue, S. G. Greenbaum, *Journal of Electroanalytical Chemistry,* **491**, pp. 203-210, (2000).

[12] D. Golodnitsky, E. Livshits, E. Peled, *Macromol. Symp,* **203**, pp. 27-45, (2003).

[13] D. Golodnitsky, E. Peled, E. Livshits, A. Ulus, Z. Barkay, I. Lapides, S. H. Chung, Y. Wang, S. G. Greenbaum, *Journal of Physical Chemistry*, part A, **105**, pp. 10098-10106, (2001).

[14] D. Golodnitsky, E. Peled, E. Livshits, I. Lapides, Yu. Rozenberg, S. H. Chung, Y. Wang, S. G. Greenbaum, *Solid State Ionics,* **147**, pp. 265-273, (2002).

[15] V. Kuppa and E. Manias, *Chem. Mater.* **14**, pp.2171-2175, (2002).

[16] B. Hille, *Ionic Channels of Excitable Membranes,* Sinauer and Assoc., NY 1993.

[17] R. S. Eisenberg, *Contemp. Phys.* **39**, pp. 447-466 (1998).

[18] Z. Schuss, B. Nadler and R. S. Eisenberg, *Phys. Rev. E* **64** (2-3) 036116, pp. 1-14, (2001).

[19] S. Selberherr, *Analysis and Simulation of Semiconductor Devices,* Springer Verlag, NY 1984.

[20] Z. Schuss, *Theory and Applications of Stochastic Differential Equations,* Wiley, NY 1980.

[21] A. Aabloo and J. Thomas, *Solid State Ionics* **143**, pp. 83-87, (2001).

[22] B. A. Ferreira, A. T. Bernardes and W. B. De Almeida, *Journal of Molecular Structure (Theochem)* **539**, pp.93-99 (2001).

[23] H. Tadokoro, *Journal Polym. Sci. C*, Copyright (1966), John Wiley and Sons, Inc.

[24] J. D. Jackson, *Classical Electrodynamics,* 2nd edition, Wiley, NY 1975.

[25] H. Kramers, *Brownian motion in a field of force,* Physica(Utrecht) **7**, pp. 284 (1940).

[26] J.R. Macallum, C.A. Vincent (Eds.), *Polymer Electrolyte Review I,* Elsevier Applied Science, London,(1989), p. 350.

[27] J.R. Macallum, C.A. Vincent (Eds.), *Polymer Electrolyte Review I,* Elsevier Applied Science, London,(1989), p. 340.

[28] F.M. Gray, *Solid Polymer Electrolytes,* VCH, New York, (1991), p. 245.

[29] F.M. Gray, M. Armand, *Polymer Electrolytes in Handbook of Battery Materials*, Ed.: J. O. Besenhard, Wiley-VCH, 1999, 499-520.

[30] L. Greengard, V. Rokhlin, J. Comput. Phys. **73**, pp. 325 ((1987).